

Multiparametric profiling of cellular lipid metabolism in hypercholesterolemia

Simon G. Pfisterer^{1*}, PhD, Ivonne Brock^{1,2,3}, PhD, Kristiina Kanerva^{1,2,3}, PhD, Iryna Hlushchenko¹, PhD, Lassi Paavolainen⁴, PhD, Pietari Ripatti⁴, MD, Mohammad M. Islam¹, Aija Kyttälä⁵, PhD, Maria D. Di Taranto^{6,7}, PhD, Annalisa Scotto di Frega⁷, Giuliana Fortunato^{6,7}, MD, Johanna Kuusisto⁸, MD, Peter Horvath^{4,9}, PhD, Samuli Ripatti^{4,10,11}, PhD, Markku Laakso⁸, MD PhD, Elina Ikonen^{1,2,3*}, MD PhD

Affiliations:

1) Department of Anatomy, Faculty of Medicine, University of Helsinki, Helsinki, Finland; **2)** Stem Cells and Metabolism Research Program, Faculty of Medicine, University of Helsinki, Helsinki, Finland; **3)** Minerva Foundation Institute for Medical Research, Helsinki, Finland; **4)** Institute for Molecular Medicine Finland (FIMM), HiLIFE, University of Helsinki, Helsinki, Finland; **5)** Finnish Institute for Health and Welfare (THL), THL Biobank, Helsinki, Finland; **6)** Department of Molecular Medicine and Medical Biotechnologies, University of Naples Federico II, Italy; **7)** CEINGE Biotechnologie Avanzate scarl Naples, Italy; **8)** Department of Medicine, University of Eastern Finland and Kuopio University Hospital, Kuopio, Finland; **9)** Biological Research Center, Szeged, Hungary; **10)** Department of Public Health, Clinicum, Faculty of Medicine, University of Helsinki, Helsinki, Finland; **11)** The Broad Institute of MIT and Harvard, Cambridge, MA, USA, *corresponding authors.

Short title: Imaging blood cell lipid metabolism

Corresponding authors: Dr. Simon Pfisterer and Dr. Elina Ikonen, Haartmaninkatu 8, 00290

Helsinki, Finland, email: simon.pfisterer@helsinki.fi and elina.ikonen@helsinki.fi

Total word count: 7874 of 8000

Subject codes: Imaging, Lipids and Cholesterol, Cell Biology, Mechanisms,

Hypercholesterolemia

Abstract:

Rationale: Identification of cellular defects underlying the development of hypercholesterolemia in individual persons remains challenging. Quantification of low-density lipoprotein (LDL) uptake can be used to characterize the effects of LDL receptor (LDLR) variants. However, a systematic assessment of LDL uptake in healthy individuals, persons with increased polygenic risk, or carriers of identical LDLR mutations is lacking. Furthermore, establishment of additional quantitative parameters related to lipid storage might provide deeper insight into the disease.

Objective: We aimed to establish a scalable analysis pipeline enabling reliable quantification of LDL uptake and lipid storage in primary cells, to elucidate defects underlying hypercholesterolemia in individual patients.

Methods: We set up a multiparametric imaging platform for the quantification of lipid uptake and storage in cytoplasmic droplets of leukocyte populations from peripheral blood. We defined a new quantifiable parameter, cellular lipid mobilization, describing the efficiency at which cells deplete their lipid reservoirs.

Results: The 65 individuals studied, including heterozygous familial hypercholesterolemia (He-FH) patients with identical LDL receptor mutations, showed distinct profiles of LDL uptake and lipid mobilization. LDL uptake was lower in individuals with higher body mass index (BMI). Lipid mobilization correlated positively with LDL uptake and negatively with hypercholesterolemia, BMI and age. He-FH patients with remaining hypercholesterolemia despite statin treatment displayed low LDL uptake and lipid mobilization, suggesting that these readouts may help to pinpoint individuals in need of more effective lipid lowering regimen.

Moreover, their combination with a polygenic risk score for LDL cholesterol (LDL-c) explained hypercholesterolemia better than the genetic risk score alone.

Conclusions: This study highlights the heterogeneity of hypercholesterolemia aetiology in individual patients and demonstrates regulation of intracellular lipid storage as a novel quantifiable parameter in the disease. The cell-based assays established are compatible with a high-throughput format and have potential for improving personalized management of hypercholesterolemia.

Non-standard Abbreviations and Acronyms:

Apo-B: Apolipoprotein-B; BSA: Bovine serum albumine; EBV: Epstein-Barr virus; CI: Confidence interval; CVD: Cardiovascular disease; DAPI: Diamidino-2-phenylindole; DiI: 1,1'-dioctadecyl-3,3,3',3'-tetramethyl-indocarbocyanine perchlorate; DMSO: Dimethyl sulfoxide; FBS: Fetal bovine serum, FH: Familial hypercholesterolemia; Int: intensity; HEPES: 4-(2-hydroxyethyl)-1-piperazineethanesulfonic acid; LD: Lipid droplet; LDL: Low-density lipoprotein; LDL-PRS: LDL Polygenic risk score; LDLR: Low-density lipoprotein receptor; LPDS: Lipoprotein deficient serum; Ly: lymphocyte; Mo: monocyte; No: number; PBMC: Peripheral blood mononuclear cells; PBS: Phosphate buffered saline; PCSK9: Proprotein convertase subtilisin/kexin type 9; PDL: Poly-D-lysine; VLDL: Very low-density lipoprotein

Introduction:

Hypercholesterolemia is one of the most common metabolic disorders and a major risk factor for cardiovascular disease (CVD). It is characterized by an accumulation of low-density lipoprotein (LDL) cholesterol (LDL-c) in the blood¹. In familial hypercholesterolemia (FH), mutations, most commonly in the LDL receptor (*LDLR*) gene, lead to increased LDL-c. However, FH represents only 2.5% of all hypercholesterolemia patients. For the remainder, polygenic and lifestyle effects appear as the main contributing factors²⁻⁵.

Several pharmacological treatments are available for hypercholesterolemia. These include statins, ezetimibe, PCSK9 inhibitors and their combinations⁶. Statins are the first line medication, but more than 30% of statin-recipients require additional treatments^{7,8}. At present, most high-risk hypercholesterolemia patients do not achieve their LDL-c target levels, leaving them at increased risk for CVD⁹. Improved identification of patients requiring more effective cholesterol lowering treatments than statin will be pivotal to reduce CVD burden, justifying more expensive drugs for more defined patient groups. In cancer therapy cell-based assays are increasingly used to identify the best treatment option for individual patients¹⁰. However, comparable approaches are not developed to a similar degree in the management of hypercholesterolemia.

The currently available cell-based assays for hypercholesterolemia are quantification of cellular LDL uptake or LDLR cell surface expression. These readouts have been mostly utilized to characterize the severity of LDLR mutations in FH patients^{11,12}. LDLR surface expression and LDL uptake are highly variable among FH patients, including individuals carrying identical mutations¹³⁻¹⁵. This not only speaks for the importance of functional cell-based assays but also

calls for new cellular readouts to better characterize the heterogeneity of lipid metabolism in individual subjects.

LDLR expression and cellular LDL internalization are tightly regulated. Low cholesterol levels in the endoplasmic reticulum (ER) signal cholesterol starvation and trigger increased LDLR expression, while high cholesterol in the ER downregulates LDLR expression. Excess cholesterol and fatty acids are stored in lipid droplets (LD) connected to the ER, from where they can be mobilized upon need^{16,17}. We therefore considered that quantification of cellular LDs and their dynamic changes may provide additional information for assessing the cellular basis of hypercholesterolemia.

Here, we established sensitive and scalable analyses for automated quantification of fluorescent lipid uptake and storage in primary lymphocyte and monocyte populations, and defined lipid mobilization as a novel parameter measuring how efficiently cells deplete their lipid stores. We found that individuals showed marked differences in cellular lipid uptake, storage and mobilization. Lipid mobilization was lower in persons with hypercholesterolemia, increased body mass index (BMI) or age. We demonstrate the potential of lipid uptake and mobilization scores in distinguishing responsiveness to statin therapy and in improving risk assessment in hypercholesterolemia.

Methods:

Materials: Lipoprotein deficient serum (LPDS) was obtained from fetal bovine serum by ultracentrifugation as described¹⁸. For DiI-LDL, we first prepared fresh LDL from human plasma samples (Finnish Red Cross permit 39/2016) by density centrifugation¹⁹ and then labelled LDL with 1,1'-dioctadecyl-3,3,3',3'-tetramethyl-indocarbocyanine perchlorate (DiI) as described²⁰. 4',6-diamidino-2-phenylindole (DAPI), Poly-D lysine (PDL) and Histopacque Premium were obtained from Sigma. DiI, anti-mouse Alexa 568, HCS CellMask Deep Red and HCS CellMask Green were obtained from Thermo Fisher. Mouse anti-LDLR (clone 472413) was from R&D systems.

Peripheral blood mononuclear cells (PBMC) and blood samples: All blood samples were collected in accordance with the declaration of Helsinki regarding experiments involving humans. He-FH patients were identified in the Metabolic Syndrome in Men study (METSIM)²¹ and blood samples obtained during patient follow-up. Two He-FH patients (Cys325Tyr and Ser580Phe) for which we obtained PBMC and EBV lymphoblast samples were described previously²². PBMC samples from the Finnish population survey, FINRISK 2012, and the donor linked data (including genotypes) were obtained from THL Biobank (www.thl.fi/biobank) and used under the Biobank agreements no 2016_15, 2016_117 and 2018_15. The FINRISK 2012 study groups consisting of donors with elevated LDL-c levels (LDL > 5 mM, hLDL-c) and normal levels (LDL-c 2.0-2.5 mM, nLDL-c) were age, gender and BMI matched. The donors in neither of groups had cholesterol lowering medication by the time of sampling, and based on a food frequency questionnaire, did not receive an elevated proportion of energy intake as

saturated or trans-fat. Buffy coat samples from healthy blood donors were obtained from the Finnish Red Cross (permit 392016). Three healthy volunteers donated blood samples on two consecutive days after overnight fasting, to assess the intraindividual variation of LDL uptake and lipid mobilization.

Cell culture: Control EBV lymphoblasts (GM14664) were obtained from Coriell Cell Repository and cultured in RPMI-1640 supplemented with 15% FBS, penicillin/streptomycin (100 U/ ml each) and 2 mM L-Glutamine. For continuous culturing of EBV lymphoblasts, 3×10^6 cells were transferred to 5 ml of fresh medium once a week. Cells were cryopreserved in 70% PBMC medium (RPMI-1640, penicillin/streptomycin, 2 mM L-glutamine, 1 mM sodium pyruvate, and 1 mM HEPES), 20% FBS and 10% DMSO.

PBMC isolation: Blood or buffy coat samples were mixed 1:1 with phosphate buffered saline (PBS) including 2.5 mM EDTA (PBS-E). The blood mixture was gently layered over Histopacque Premium (1.0073, for mononuclear cells) and centrifuged 40 min at 400 g. The PBMC cell layer was removed, transferred to a new 15 ml reaction tube and mixed with PBS-E. Cells were centrifuged at 400 g for 10 min and incubated in 2 ml of red blood cell lysis buffer for 1 min (155 mM NH_4Cl , 12 mM NaHCO_3 , 0.1 mM EDTA). 10 ml of PBS-E was added and cells were pelleted and washed with PBS-E. Then cells were resuspended in 5 ml PBMC medium (RPMI-1640, penicillin/streptomycin, 2 mM L-glutamine, 1 mM sodium pyruvate, and 1 mM

HEPES), counted, pelleted and resuspended in freezing medium (70% PBMC-medium, 20% FBS, 10 % DMSO) and cryopreserved in liquid nitrogen.

Cell treatments, DiI-LDL uptake, transfer to imaging plates and fixation: Cryopreserved EBV lymphoblasts or PBMCs were thawed in PBMC medium, and centrifuged at 400 g for 10 min. The cells were resuspended in PBMC medium and transferred to a well of a 96 well plate (200 000 cells per well), containing FBS (10% final concentration) or LPDS (5% final concentration) and incubated for 24 h. Cells were then incubated with freshly thawed DiI-LDL at 30 µg / ml final concentration for 1 h at 37°C, which yielded an optimal signal intensity at a linear detection range in PBMCs. Subsequently, cells were transferred to conical 96 well plates and centrifuged at 400 g for 10 min. Using a robotic platform (Opentrons, New York, USA) medium was removed and cells were resuspended in PBMC medium. Cells were centrifuged, automatically resuspended in PBMC medium and transferred to PDL coated 384 well high-content imaging plates (approximately 40 000 cells per well, a density where individual cells are not on top but close to each other). After 30 min of incubation at 37°C cells were automatically fixed with 4% paraformaldehyde in 250 mM HEPES, 1 mM CaCl₂, 100 µM MgCl₂, pH 7.4 and washed with PBS. For lipid droplet and LDLR surface stainings, cells were directly transferred to PDL coated 384 well high-content plates, adhered, automatically fixed and washed with PBS.

Lipid droplet analyses: Cells were processed as described before²⁷ with the following changes: Fixed cell samples were automatically stained with 1 µg/ml LD540 (Princeton BioMolecular

Research) and 5 $\mu\text{g}/\text{ml}$ DAPI. 3D stacks of optical slices were acquired automatically either with a Nikon Eclipse Ti-E inverted microscope equipped with a 40 \times Planfluor objective with NA 0.75 and 1.5 zoom; duplicate wells, each with six image fields per patient, or with a PerkinElmer Opera Phenix High Content Imaging system with a 63x water immersion objective, NA 1.15; duplicate wells, each with 14, 16 (two wells combined) or 24 (two wells combined) image fields. Image stacks were automatically deconvolved either with Huygens software (Scientific Volume Imaging, b.v.) or a custom-made Python tool based on the open-source tools PSF generator²³ and deconvolution lab²⁴. Maximum intensity projections were made from the deconvolved image stacks with custom Python tools. Automated quantification of lipid droplets was performed as described previously²⁵⁻²⁷.

LDLR surface staining: All staining procedures were performed automatically. Fixed cells were quenched with 50 mM NH_4Cl for 15 min and washed twice with PBS. Cells were incubated with block solution (PBS, 1% BSA) for 10 min followed by staining with mouse anti-LDLR in block solution for 60 min. Cells were washed three times with PBS followed by incubation with secondary antibody solution (anti-mouse-Alexa 568, DAPI 5 $\mu\text{g}/\text{ml}$ and HCS CellMask Green stain 0.25 $\mu\text{g}/\text{ml}$) for 45 min at room temperature. Cells were washed with PBS and 3D stacks of optical slices were acquired for DAPI (nuclei), CellMask Green (cytoplasm), Alexa 568 (LDLR surface) and Alexa 640 (background) channels using an Opera Phenix high-content imaging system with a 40x water immersion objective NA 1.1; quadruplicate wells, each with seven image fields per patient. LDLR surface and background images were automatically deconvolved with our custom build Python deconvolution tools and maximum intensity projections were

made. The resulting images were automatically analysed with CellProfiler²⁸. LDLR surface intensities were background subtracted for each individual cell and normalized by subtracting mean LDLR surface intensities from the two controls, which were included in each imaging plate.

Quantification of DiI-LDL uptake: DiI-LDL labeled, and fixed cells (see section cell treatments) were automatically processed with a robotic platform (Opentrons). Cells were stained with 5 µg/ml DAPI and 0.5 µg/ml HCS CellMask Deep Red and image stacks for three channels, DAPI (nuclei), DiI-LDL and CellMask Deep Red (cytoplasm) were acquired. Automated microscopy and single cell quantifications with CellProfiler were performed as described in the section LDLR surface staining; Quadruplicate wells, each with 7 image fields for heterozygous FH patients; duplicate wells, each with 13 image fields for FINRISK subjects. Plate effects were determined with control samples and corrected for in the individual experiments.

LDL polygenic risk score (LDL-PRS): We calculated the LDL PRS using the LDpred method based on both an European genome-wide association study (GWAS) meta-analysis with 56945 samples and the previously published PRS by *Talmud et al.*^{4,29}. The PRS calculation is described in greater detail in the supplementary methods section. LDL uptake and lipid mobilization parameters were normalized to a range from 0 to 1 to generate uptake and mobilization scores. Hybrid scores represent the average of LDL-PRS and uptake and/or mobilization scores which were normalized to a range from 0 to 1.

Data analysis: Segmented images from CellProfiler underwent routine visual controls to verify cell identification and filter out potential imaging artifacts. Then, Lymphocytes and monocytes were detected based on the size of the cytoplasm (Ly <115 μm^2 , Mo >115 μm^2) (See Suppl. Figure 1). We averaged the cellular mean DiI-LDL intensities and organelle counts for each cell population and well and normalized them to the average of both controls included in each plate, set to 100%. For LD quantifications we first selected monocytes with at least one LD. We then averaged cellular LD number and total LD area (LD number x LD size) for each well. For lipid mobilization we first averaged the control medium results for LD-Pos, LD-No, and LD-area from duplicate wells and then divided these by the respective per well results after lipid starvation. We used Python (Python Software Foundation, www.python.org) with the following packages to perform the single cell data analysis (Pandas, Numpy, Scipy, Matplotlib³⁰, Seaborn³¹). For statistical significance testing we first performed Levene's test to assess the equality of sample variation. For equal sample amounts and variance, we performed two-tailed Student's t-test. For unequal samples or variance, we utilized Welch's t-test. For correlations we first performed a linear regression of the two measurements and then calculated a two-sided p-value for a hypothesis test whose null hypothesis is that the slope is zero, using Wald Test with t-distribution of the test statistic. Fisher's exact probability test was used to calculate the odds ratio.

Data and code availability: The data that support the findings of this study are available from the authors upon request. Genetic data for the subjects of the FINRISK cohort study is available

from the THL Biobank (<https://thl.fi/en/web/thl-biobank>). Custom python tools for image processing and deconvolution are available her: These tools can be accessed via:

<https://github.com/lopaavol/Oputils>. Software tools for lipid droplet detection have been described previously²⁷ and are available via:

<https://bitbucket.org/szkabel/lipidalyzer/get/master.zip>

Results:

Automated pipeline for quantification of hypercholesterolemia-related functional defects in primary human leukocytes

Several cell types such as lymphocytes, monocytes and Epstein-Barr virus (EBV) immortalized lymphoblasts have been used for measuring LDL uptake^{32,33}, but assays based on fluorescent LDL suffered from low sensitivity. Whilst EBV lymphoblasts show the highest LDL uptake, cell immortalization is time consuming and alters cellular functions^{32,34}. We therefore set up an automated imaging and analysis pipeline for sensitive quantification of LDL uptake and LDLR surface expression from less than two million peripheral blood mononuclear cells (PBMCs) (2-4 ml blood) (**Figure 1A**). Cryopreserved PBMCs were recovered in 96 well plates at defined densities and incubated with lipid-rich control medium (CM, 10% FBS) or lipid poor medium (LP, 5% lipoprotein-deficient serum) for 24 h. Cells were labelled with fluorescent LDL particles (DiI-LDL) for 1 h, washed and automatically transferred to 384 well plates for staining and automated high-content imaging (**Figure 1A**). After adhesion to coated imaging plates, lymphocytes remain small while monocytes spread out, enabling identification of leukocyte populations based on size: PBMCs with a cytoplasmic area $<115 \mu\text{m}^2$ were classified as lymphocytes and those with a cytoplasmic area $>115 \mu\text{m}^2$ as monocytes (**Suppl. Figure 1A-C**).

In CM, DiI-LDL uptake into lymphocytes and monocytes was more than two-fold above the background of non-labeled cells (**Figure 1B-D**). Lipid starvation further increased DiI-LDL uptake in both cell populations (**Figure 1C, D**). We aggregated the single-cell data from individual wells and averaged the results from 2-4 wells for each treatment, enabling the quantification of about 700 monocytes and 2300 lymphocytes per well (**Suppl. Figure 1D**). For

both cell populations, we defined two readouts, cellular DiI-LDL intensity (DiI-Int), reflecting DiI-LDL surface binding and internalization, and DiI-LDL organelle number (DiI-No), reflecting internalized DiI-LDL (**Fig 1E, F**). This results in four parameters: monocyte (Mo) DiI-Int, lymphocyte (Ly) DiI-Int, Mo DiI-No and Ly DiI-No. In both cell populations, DiI-Int was inhibited by adding surplus unlabeled LDL, arguing for a saturable, receptor-mediated uptake mechanism (**Suppl. Figure 1E**).

In lipid rich conditions, Mo DiI-Int was slightly higher than Ly DiI-Int (**Figure 1E**), and upon lipid starvation, Mo DiI-Int increased more profoundly, providing a larger fold increase than Ly DiI-Int (**Figure 1E**). Furthermore, Mo DiI-No was roughly ten-fold higher than Ly DiI-No, with both parameters showing a five-fold increase upon lipid starvation (**Figure 1F**). Thus, DiI-LDL uptake into monocytes is better than into lymphocytes, but both cell populations respond to lipid starvation. As EBV lymphoblasts are often a preferred choice for LDL uptake studies²⁰ we compared LDL uptake between EBV lymphoblasts and monocytes (**Suppl. Figure 1F,G**). This showed that DiI-Int signal intensity after lipid starvation was roughly similar in EBV-lymphoblasts and monocytes, implying that the primary cells provide high enough DiI-LDL signal intensities without time consuming cell immortalization (**Suppl. Figure 1G**).

To enable data comparison between experiments, we included two controls. Each control consisted of a mixture of large-scale PBMC isolations from four healthy blood donors, with the cells cryopreserved at a defined density for one-time use aliquots. In each experiment, Mo DiI-Int, Ly DiI-Int, Mo DiI-No and Ly DiI-No were normalized to these controls. We also introduced a combinatorial score, pan-LDL uptake (or pan-uptake), representing the average of Mo DiI-Int, Ly DiI-Int, Mo DiI-No and Ly DiI-No. We then assessed the intraindividual variability of these

five readouts in three individuals on two consecutive days (**Suppl. Figure 1H**). The intraindividual variability was low for a cell-based assay, especially in monocytes, with 7.6% for Mo DiI-No, 12% for Mo DiI-Int and 13% for pan-uptake. The values were only moderately higher in lymphocytes, with DiI-Int 15% and DiI-No 21.1% (**Suppl. Figure 1I**).

We next validated our LDL uptake measurements in PBMCs of two He-FH patients (Cys325Tyr and Ser580Phe mutations in *LDLR*) with highly elevated LDL-c, and reduced LDL uptake in EBV lymphoblasts (**Suppl. Figure 1J**). For both patients, Mo and Ly DiI-No as well as Mo DiI-Int were reduced by more than 45%, Ly DiI-Int was less profoundly decreased, and pan-uptake was reduced by over 50% (**Figure 1G, H; Suppl. Figure 1J**). Together, these data indicate that our analysis pipeline enables quantification of multiple LDL uptake parameters in major leukocyte cell populations and distinguishes defective *LDLR* function therein.

Heterogeneous LDL uptake and LDLR surface expression in He-FH patients

We next used our analysis pipeline to characterize 21 He-FH patients from the Metabolic Syndrome in Men (METSIM) cohort study²¹ (**Suppl. Table 1**). The patients' mutations are localized in the *LDLR* coding region, ranging from pathogenic to likely benign variants (**Figure 2A**). Quantification of DiI-Int and DiI-No for monocytes and lymphocytes provided highly similar results for each person (**Figure 2B**). However, there were substantial interindividual differences for the LDL uptake parameters, also between persons harboring identical *LDLR* mutations (**Figure 2B**). This was most pronounced for FH-North Karelia (Pro309Lysfs*59), a pathogenic loss of function variant, but also evident for FH-Pogosta (Arg595Gln) and FH-

Glu626Lys (**Figure 2A, B**). These observations imply that in He-FH, regulatory mechanisms may enhance the expression of the unaffected *LDLR* allele and/or stabilize the encoded protein. In support, we obtained a strong correlation between monocyte LDLR surface expression and DiI-Int, DiI-No and pan-uptake scores for the same individuals (pan-uptake, $R=0.58$, $p=0.006$), (**Figure 2C, Suppl. Figure 2A**).

Interestingly, the pan-uptake score showed a tendency for lower values in FH-North Karelia variants as compared to the likely pathogenic FH-Pogosta and likely benign Glu626Lys variants (**Suppl. Figure 2B**). This is in agreement with higher LDL-c concentrations in FH-North Karelia patients³⁵. While LDL uptake did not correlate with circulating LDL-c for the entire study group (**Suppl. Figure 2C**), this correlation was highly significant for monocyte DiI-Int, DiI-No and the pan-uptake scores for the 11 He-FH patients on statin monotherapy (Mo DiI-Int: $R=-0.75$, $p=0.0081$, **Figure 2D**). Importantly, 3 of the individuals with the lowest monocyte DiI-Int had a two-fold higher LDL-c concentration than the 3 with the highest monocyte DiI-Int (**Figure 2E**).

LDL uptake in non-FH individuals with normal or elevated blood LDL-c

Most hypercholesterolemia patients do not carry *LDLR* mutations². We therefore investigated cellular LDL uptake in PBMCs from 20 biobank donors with elevated LDL-c levels (LDL-c >5 mM) (hLDL-c) and from 19 donors with normal LDL levels (LDL-c 2-2.5 mM) (nLDL-c) from the FINRISK population cohort³⁶ (**Suppl. Table 2**). DNA sequencing confirmed that common Finnish *LDLR* variants were not present among these subjects.

We quantified DiI-Int and DiI-No for monocyte and lymphocyte populations as well as the pan-uptake score for nLDL-c and hLDL-c individuals. This revealed a large interindividual variability in LDL uptake (**Figure 3A**). Both groups included persons with severely reduced LDL internalization, but the lowest pan-LDL uptake scores were among the hLDL-c individuals (**Figure 3A**). Overall, pan-uptake and Ly DiI-No were reduced in hLDL-c compared to nLDL-c subjects, but the differences were not significant (**Suppl. Figure 3A, B**). Of note, reduced pan-uptake, Mo DiI-Int and Ly DiI-No correlated with increased blood LDL-c levels in the hLDL-c subgroup, but the correlations relied on a single individual with a very high blood LDL-c concentration (**Suppl. Figure 3C**).

To investigate additional factors influencing the interindividual variability in cellular LDL uptake, we analyzed correlations to two obesity indicators, body mass index (BMI) and waist circumference. Strikingly, reduced pan-uptake, as well as Mo DiI-Int and Ly DiI-Int correlated with increased waist circumference (pan-uptake: $R=-0.42$, $p=0.009$; **Figure 3B**). Lower pan-uptake, Ly DiI-Int and Mo DiI-Int also correlated with elevated BMI (pan-uptake: $R=-0.36$, $p=0.022$; **Figure 3C**).

Assessment of cellular lipid storage and mobilization in leukocytes

Cells store excess lipids in LDs and this is related to lipid uptake: When peripheral cells have sufficient lipids available, they typically exhibit LDs and in parallel, lipid uptake is downregulated. We therefore also included the staining of LDs in the automated analysis pipeline(**Figure 1A**). Staining of PBMCs in lipid rich conditions (CM) with the LD dye LD540

revealed that lymphocytes and monocytes displayed LDs in a heterogenous fashion (**Figure 4A**), with lymphocytes showing fewer LD positive cells and fewer LDs per cell than monocytes (**Figure 4B, C**). We then visualized the changes in LD abundance upon overnight lipid starvation (LP) (**Figure 4B-F**). This resulted in a pronounced decrease in lipid deposition: In CM, 9% of lymphocytes and 25% of monocytes contained LDs, but upon lipid starvation, these were reduced to 6% (Ly) and 12% (Mo) (**Figure 4D**).

Due to the lower LD abundance in lymphocytes, we focused on monocytes and defined three readouts for them: 1) Percentage of LD-positive cells (LD-Pos), 2) Cellular LD number in LD-Pos (LD-No) and 3) Total cellular LD Area in LD-Pos (LD-Area). On average, LD-Pos cells showed 2.9 LDs in lipid rich conditions and 1.8 LDs upon lipid starvation (**Figure 4E**). The total LD area decreased from $1.35 \mu\text{m}^2$ in lipid rich conditions to $0.8 \mu\text{m}^2$ upon lipid starvation (**Figure 4F**).

When quantifying LD parameters from several subjects, we observed substantial differences between individuals in how LDs changed upon lipid starvation. To systematically quantify these differences, we established a parameter, lipid mobilization score, that reflects how efficiently cellular lipid stores are depleted under lipid starvation (**Figure 4G**). Lipid mobilization scores were calculated for each of the LD readouts, LD-Pos, LD-No and LD-Area, by dividing the results obtained in lipid rich conditions with those obtained after lipid starvation (**Figure 4G**). Furthermore, we established a pan-mobilization score by averaging LD-Pos, LD-No and LD-Area scores (**Figure 4G, H**), with LD-Pos providing the highest mobilization score but also the highest variability (**Figure 4H**).

To further assess the reliability of the LD mobilization parameters, we determined their intraindividual variation using the same samples as for analyzing intraindividual variation of DiI-LDL uptake (**Suppl. Figure 1I, J**). This showed a modest intraindividual variation for the lipid mobilization scores (**Suppl. Figure 4A**), which was on average 8% for pan-mobilization, 10% for LD-Pos, 11% for LD-No and 13% for LD-Area (**Suppl. Figure 4B**).

Cellular lipid mobilization in He-FH patients

When lipid mobilization was analyzed from the He-FH samples of the METSIM cohort, we found that the pan-mobilization score was significantly reduced in He-FH individuals carrying the FH-North Karelia and Glu626Lys variants (**Figure 4I**). This suggests that defective LDLR function may be accompanied by reduced lipid mobilization. We also studied whether the combination of a lipid mobilization score with LDL uptake improves identification of statin recipients with high residual LDL-c concentrations. Several of the patients with intermediate and high LDL-c showed low monocyte DiI-LDL intensities in a narrow range (**Figure 2D**). When monocyte DiI-Int was combined with the pan- mobilization score, larger differences between patients were observed, providing a better separation of individuals with high and intermediate LDL-c (**Figure 4J**). Moreover, the difference in LDL-c concentration between 3 individuals with the highest vs. lowest score was more significant than when using monocyte DiI-Int alone (**Figure 4K vs. Figure 2E**).

Cellular lipid mobilization is reduced in non-FH hypercholesterolemia patients and correlates with LDL uptake

We then investigated whether monocytes from nLDL-c and hLDL-c biobank donors displayed differences in lipid mobilization. Analogously to LDL uptake, we observed a large variability for the pan- and individual mobilization scores in this cohort (**Figure 5A**). Interestingly, pan-mobilization, LD-No and LD-Area were significantly reduced in the hLDL-c compared to nLDL-c subjects (**Figure 5A, B, Suppl. Figure 5A, B**). This prompted us to scrutinize whether lipid mobilization correlates with LDL uptake related parameters or obesity indicators in this cohort. All mobilization scores correlated positively with the pan-uptake score ($R=0.42$, $p=0.0095$ for pan-mobilization; **Figure 5C**). Furthermore, pan-, LD-No and LD-Area mobilization scores correlated negatively with total cholesterol and apo-B concentrations (**Suppl. Figure 5C, D**). Remarkably, the pan-mobilization score correlated negatively with BMI ($R=-0.34$, $p=0.036$; **Figure 5D**) and LD-No, and LD-Area were negatively correlated with waist circumference ($R=-0.32$, $p=0.0495$ for LD-No; **Suppl. Figure 5E**). Moreover, higher LD-No, LD-Area and pan-mobilization scores correlated negatively with age ($R=-0.38$, $p=0.019$ for pan-mobilization; **Figure 5E**).

Hybrid scores of genetic and functional cell data show improved association with hypercholesterolemia

The hLDL-c biobank donors of the FINRISK population cohort displayed an increased LDL-polygenic risk score (LDL-PRS) (**Figure 6A**). LDL-PRS did not correlate with LDL uptake or lipid mobilization (**Suppl. Figure 6A, B**), suggesting that LDL-PRS and cellular LDL uptake monitor at least in part distinct processes. Interestingly, combination of LDL-PRS with pan-uptake reduced the variation and made it easier to discriminate nLDL-c and hLDL-c populations, providing an eight times better p-value as compared to LDL-PRS only (**Figure 6B**).

Furthermore, combination of the pan-mobilization score with LDL-PRS drastically improved the discrimination of both groups (**Figure 6C**) and combining all three parameters, i.e. LDL-PRS, pan-uptake and pan-mobilization, provided the best discrimination power and lowest p-value, 60-fold better than LDL-PRS alone (**Figure 6D**). To estimate the association of LDL-PRS and novel hybrid scores with elevated LDL-c (>5 mmol/l), we calculated the odds ratio (OR) for elevated LDL-c by comparing individuals with the highest 30% of the score to the remaining subjects. Combining LDL-PRS either with pan-uptake or pan-mobilization doubled the OR and using the hybrid score combining all three readouts resulted in a five-fold higher OR (**Figure 6E**).

Discussion

In this study, we established a multiplexed high-content analysis pipeline to quantify lipid uptake and storage in primary lymphocyte and monocyte populations, analyzing over 310 conditions (combinations of assays and treatments) from 65 patient samples. Overall, besides automation of cell handling, staining and imaging procedures enabling high-throughput applications, this platform provides significant advantages over existing methodologies to assess the lipid status in PBMCs: Immobilization of cells to coated surfaces allows image acquisition after sample storage and subcellular imaging resolution enables quantification of internalized LDL as well as LDs.

We observed highly divergent LDL uptake and LDLR surface expression patterns in He-FH individuals carrying identical *LDLR* mutations. This argues that the *LDLR* genotype is not a uniformly dominant determinant of cellular LDL uptake. Nevertheless, high LDL uptake correlated with low circulating LDL-c for He-FH patients on statin treatment. This is in line with previous observations using radioactive LDL^{37,38}. We also found a marked variability in cellular LDL uptake in individuals who did not carry common Finnish FH mutations, irrespective of their LDL-c levels. This prompted us to search for additional imaging-based readouts to compare lipid handling between individuals and to better explain the variation in LDL-c in the population. We established a new parameter, lipid mobilization score, that is based on the detection of LD-related parameters in lipid-rich and -poor conditions and quantifies the consumption of LDs during starvation.

Increased lipid mobilization correlated with increased LDL uptake, implying that efficient removal of cellular lipids is typically paralleled by efficient lipid uptake. Importantly, in the FINRISK population cohort, lipid mobilization outperformed LDL uptake in distinguishing

individuals with high (>5 mmol/l) and normal LDL-c (2-2.5 mmol/l), with impaired lipid mobilization associating with elevated LDL-c. Therefore, lipid mobilization highlights additional aspects of cellular lipid metabolism underlying hypercholesterolemia in individual patients.

Obesity associated metabolic syndrome is typically linked to dyslipidemia characterized by decreased high-density lipoprotein cholesterol (HDL-c), elevated LDL-c with increased small dense LDL particles and increased fasting plasma triglycerides³⁹. We found that increased BMI and waist circumference correlated with reduced LDL uptake and lipid mobilization. This suggests that defective LDL clearance contributes to dyslipidemia in overweight individuals. Accordingly, LDLR expression has been reported to be reduced in obese subjects⁴⁰. Furthermore, our data argue that reduced lipid mobilization may underlie the decreased LDL uptake and represent one of the cellular hallmarks of metabolic dysregulation in obesity.

Moreover, by combining LDL uptake and lipid mobilization parameters for He-FH patients on statin therapy, it was easier to pinpoint individuals with remaining high LDL-c. This suggests that the analyses help to identify He-FH cases that remain refractory to statin monotherapy. Although radiolabeled LDL uptake measurements already pointed to this direction^{37,38}, the assays described here are much better compatible with a high-throughput format. Thus, they may have potential for stratifying patients that will require additional, more expensive treatments, such as PCSK9 inhibitors.

Polygenic risk scores (PRS) provide tools for cardiovascular risk profiling and are increasingly included in clinical care guidelines of hypercholesterolemia^{1,6}. Hypercholesterolemic subjects of the FINRISK cohort showed an increased LDL-PRS, but this did not correlate with LDL uptake or lipid mobilization, arguing that the cell functional parameters cover in part different territories

than PRS. We therefore investigated if combining LDL-PRS and cell-based data improves the discrimination of individuals with elevated and normal LDL-c. Indeed, the combination of LDL uptake, lipid mobilization and LDL-PRS drastically improved the segregation of hyper- and normocholesterolemic subjects. An increased LDL-PRS is associated with a higher incidence of coronary artery disease⁵. As the hybrid scores of functional cell-based data and LDL-PRS efficiently increased the association with high LDL-c, we anticipate that the cell-based assays will provide valuable information for future integrated CVD risk calculations. They may facilitate the detection of hypercholesterolemia risk at younger age when clinical manifestations are not yet overt, thus enabling faster initiation of treatment and improved disease prevention⁴¹.

In summary, this study establishes automated assays for reliable quantification of lipid uptake and mobilization in human leukocytes, providing novel insights into the cellular mechanisms underlying hypercholesterolemia (**Figure 7**). We propose that these readouts may have potential to improve personalized management in hypercholesterolemia, for instance by helping to pinpoint individuals in need of treatment beyond statin monotherapy and by improving hypercholesterolemia/CVD risk assessment.

Acknowledgements:

We thank Anna Uro for technical assistance; HiLIFE and Biocenter Finland supported Helsinki BioImaging infrastructures for help with microscopy; Katariina Öörni for help with LDL preparation; Abel Szkalitsy for help with image analysis. We thank THL Biobank for providing samples and data for this study (study no: 2016_15, 2016_117 and 2018_15) and all biobank donors for their participation in biobank research.

Sources of Funding:

This study was supported by The Academy of Finland (grants 282192, 284667, 307415 to E.I.; 321428 to M.L.; 310552 to LP; 328861, 325040 to SP; and 312062, 316820 to SR), Sigrid Juselius Foundation (grant to E.I. M.L. S.R.), University of Helsinki (grant to K.K.; Faculty of Medicine early-career investigator grant to SP; HiLIFE Fellow grant to E.I.), Finnish Foundation for Cardiovascular Research and University of Helsinki HiLIFE Fellow and Grand Challenge grants, and H2020-INTERVENE (101016775) to SR, MIUR of Italy (project cod. PON03PE_00060_7, grant to CEINGE, G.F.), LENDULET-BIOMAG Grant (2018-342), H2020-discovAIR (874656), and Chan Zuckerberg Initiative (seed networks for the HCA-DVP) to PH. Ida Montin Foundation (grant to P.R.), Doctoral Programme in Population Health, University of Helsinki (grant to P.R.); Emil Aaltonen Foundation (grant to P.R.)

Disclosures:

A patent application covering the use of the here suggested patient stratification methods has been filed (Application: FI 20206284) in which University of Helsinki is the applicant and EI and SP are the inventors.

References:

1. Borén, J. *et al.* Low-density lipoproteins cause atherosclerotic cardiovascular disease: pathophysiological, genetic, and therapeutic insights: a consensus statement from the European Atherosclerosis Society Consensus Panel. *Eur. Heart J.* (2020) doi:10.1093/eurheartj/ehz962.
2. Abul-Husn, N. S. *et al.* Genetic identification of familial hypercholesterolemia within a single U.S. health care system. *Science* **354**, aaf7000 (2016).
3. Khera, A. V. *et al.* Diagnostic Yield and Clinical Utility of Sequencing Familial Hypercholesterolemia Genes in Patients With Severe Hypercholesterolemia. *Journal of the American College of Cardiology* **67**, 2578–2589 (2016).
4. Talmud, P. J. *et al.* Use of low-density lipoprotein cholesterol gene score to distinguish patients with polygenic and monogenic familial hypercholesterolaemia: a case-control study. *The Lancet* **381**, 1293–1301 (2013).
5. Ripatti Pietari *et al.* Polygenic Hyperlipidemias and Coronary Artery Disease Risk. *Circulation: Genomic and Precision Medicine* **13**, e002725 (2020).
6. Mach, F. *et al.* 2019 ESC/EAS guidelines for the management of dyslipidaemias: Lipid modification to reduce cardiovascular risk. *Atherosclerosis* **290**, 140–205 (2019).
7. Ridker, P. M., Mora, S. & Rose, L. Percent reduction in LDL cholesterol following high-intensity statin therapy: potential implications for guidelines and for the prescription of emerging lipid-lowering agents. *Eur Heart J* **37**, 1373–1379 (2016).
8. Boekholdt, S. M. *et al.* Very Low Levels of Atherogenic Lipoproteins and the Risk for Cardiovascular Events: A Meta-Analysis of Statin Trials. *Journal of the American College of Cardiology* **64**, 485–494 (2014).

9. Ray, K. K. *et al.* EU-Wide Cross-Sectional Observational Study of Lipid-Modifying Therapy Use in Secondary and Primary Care: the DA VINCI study. *European Journal of Preventive Cardiology* (2020) doi:10.1093/eurjpc/zwaa047.
10. Snijder, B. *et al.* Image-based ex-vivo drug screening for patients with aggressive haematological malignancies: interim results from a single-arm, open-label, pilot study. *Lancet Haematol* **4**, e595–e606 (2017).
11. Romano, M. *et al.* Identification and functional characterization of LDLR mutations in familial hypercholesterolemia patients from Southern Italy. *Atherosclerosis* **210**, 493–496 (2010).
12. Benito-Vicente, A. *et al.* Validation of LDLr Activity as a Tool to Improve Genetic Diagnosis of Familial Hypercholesterolemia: A Retrospective on Functional Characterization of LDLr Variants. *International Journal of Molecular Sciences* **19**, 1676 (2018).
13. Urdal, P., Leren, T. P., Tonstad, S., Lund, P. K. & Ose, L. Flow cytometric measurement of low density lipoprotein receptor activity validated by DNA analysis in diagnosing heterozygous familial hypercholesterolemia. *Cytometry* **30**, 264–268 (1997).
14. Tada, H. *et al.* A novel method for determining functional LDL receptor activity in familial hypercholesterolemia: Application of the CD3/CD28 assay in lymphocytes. *Clinica Chimica Acta* **400**, 42–47 (2009).
15. Thedrez Aurélie *et al.* Homozygous Familial Hypercholesterolemia Patients With Identical Mutations Variably Express the LDLR (Low-Density Lipoprotein Receptor). *Arteriosclerosis, Thrombosis, and Vascular Biology* **38**, 592–598 (2018).
16. Ikonen, E. Cellular cholesterol trafficking and compartmentalization. *Nat. Rev. Mol. Cell Biol.* **9**, 125–138 (2008).
17. Luo, J., Yang, H. & Song, B.-L. Mechanisms and regulation of cholesterol homeostasis. *Nat Rev Mol Cell Biol* **21**, 225–245 (2020).

18. Goldstein, J. L., Basu, S. K. & Brown, M. S. Receptor-mediated endocytosis of low-density lipoprotein in cultured cells. *Meth. Enzymol.* **98**, 241–260 (1983).
19. Stephan, Z. F. & Yurachek, E. C. Rapid fluorometric assay of LDL receptor activity by DiI-labeled LDL. *J. Lipid Res.* **34**, 325–330 (1993).
20. Reynolds, G. D. & St Clair, R. W. A comparative microscopic and biochemical study of the uptake of fluorescent and 125I-labeled lipoproteins by skin fibroblasts, smooth muscle cells, and peritoneal macrophages in culture. *Am J Pathol* **121**, 200–211 (1985).
21. Laakso, M. *et al.* The Metabolic Syndrome in Men study: a resource for studies of metabolic and cardiovascular diseases. *J. Lipid Res.* **58**, 481–493 (2017).
22. Romano, M. *et al.* An improved method on stimulated T-lymphocytes to functionally characterize novel and known LDLR mutations. *J Lipid Res* **52**, 2095–2100 (2011).
23. Kirshner, H., Aguet, F., Sage, D. & Unser, M. 3-D PSF fitting for fluorescence microscopy: implementation and localization application. *Journal of Microscopy* **249**, 13–25 (2013).
24. Sage, D. *et al.* DeconvolutionLab2: An open-source software for deconvolution microscopy. *Methods* **115**, 28–41 (2017).
25. Pfisterer, S. G. *et al.* Role for formin-like 1-dependent acto-myosin assembly in lipid droplet dynamics and lipid storage. *Nature Communications* **8**, 14858 (2017).
26. Vanharanta, L. *et al.* High-content imaging and structure-based predictions reveal functional differences between Niemann-Pick C1 variants. *Traffic* **21**, 386–397 (2020).
27. Salo, V. T. *et al.* Seipin Facilitates Triglyceride Flow to Lipid Droplet and Counteracts Droplet Ripening via Endoplasmic Reticulum Contact. *Developmental Cell* **50**, 478-493.e9 (2019).
28. Carpenter, A. E. *et al.* CellProfiler: image analysis software for identifying and quantifying cell phenotypes. *Genome Biology* **7**, R100 (2006).

29. Vilhjálmsón, B. J. *et al.* Modeling Linkage Disequilibrium Increases Accuracy of Polygenic Risk Scores. *Am. J. Hum. Genet.* **97**, 576–592 (2015).
30. Hunter, J. D. Matplotlib: A 2D Graphics Environment. *Computing in Science Engineering* **9**, 90–95 (2007).
31. Michael Waskom *et al.* *mwaskom/seaborn: v0.8.1 (September 2017)*. (Zenodo, 2017). doi:10.5281/zenodo.883859.
32. Chan, P., Jones, C., Lafrenière, R. & Parsons, H. G. Surface expression of low density lipoprotein receptor in EBV-transformed lymphocytes: characterization and use for studying familial hypercholesterolemia. *Atherosclerosis* **131**, 149–160 (1997).
33. Schmitz G, Brüning T, Kovacs E & Barlage S. Fluorescence flow cytometry of human leukocytes in the detection of LDL receptor defects in the differential diagnosis of hypercholesterolemia. *Arteriosclerosis and Thrombosis: A Journal of Vascular Biology* **13**, 1053–1065 (1993).
34. Piccaluga, P. P., Weber, A., Ambrosio, M. R., Ahmed, Y. & Leoncini, L. Epstein–Barr Virus-Induced Metabolic Rearrangements in Human B-Cell Lymphomas. *Front Microbiol* **9**, (2018).
35. Lahtinen, A. M., Havulinna, A. S., Jula, A., Salomaa, V. & Kontula, K. Prevalence and clinical correlates of familial hypercholesterolemia founder mutations in the general population. *Atherosclerosis* **238**, 64–69 (2015).
36. Borodulin, K. *et al.* Cohort Profile: The National FINRISK Study. *Int J Epidemiol* **47**, 696–696i (2018).
37. Hagemenas F C & Illingworth D R. Cholesterol homeostasis in mononuclear leukocytes from patients with familial hypercholesterolemia treated with lovastatin. *Arteriosclerosis: An Official Journal of the American Heart Association, Inc.* **9**, 355–361 (1989).

38. Hagemenas, F. C., Pappu, A. S. & Illingworth, D. R. The effects of simvastatin on plasma lipoproteins and cholesterol homeostasis in patients with heterozygous familial hypercholesterolaemia. *European Journal of Clinical Investigation* **20**, 150–157 (1990).
39. Klop, B., Elte, J. W. F. & Cabezas, M. C. Dyslipidemia in obesity: mechanisms and potential targets. *Nutrients* **5**, 1218–1240 (2013).
40. Mamo, J. C. L. *et al.* Postprandial dyslipidemia in men with visceral obesity: an effect of reduced LDL receptor expression? *American Journal of Physiology-Endocrinology and Metabolism* **281**, E626–E632 (2001).
41. Wiegman, A. *et al.* Familial hypercholesterolaemia in children and adolescents: gaining decades of life by optimizing detection and treatment. *Eur Heart J* **36**, 2425–2437 (2015).

Figures with Figure legends:

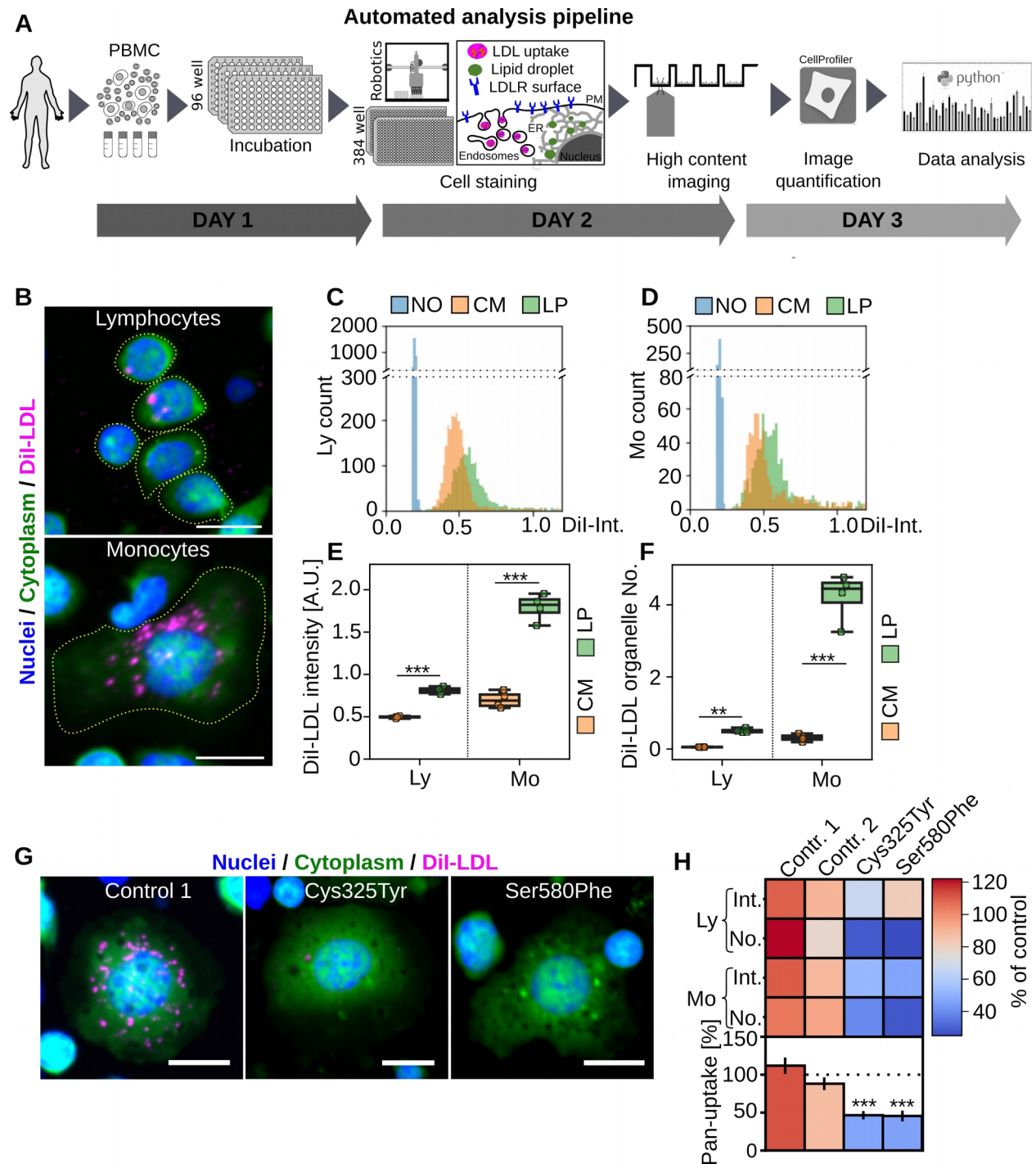


Figure 1: Automated analysis pipeline for multiplex quantification of functional

phenotypes in PBMCs. A) Schematic presentation of the automated analysis pipeline. For each experiment cryopreserved PBMC samples were thawed, aliquoted into 96 wells and incubated overnight with lipid rich (CM, 10% FBS) or lipid poor medium (LP, 5% LPDS). Cells were labeled with fluorescent LDL (DiI-LDL) or directly transferred to 384 well imaging plates, automatically fixed, stained and subjected to automated high-content imaging. Images were quantified with CellProfiler and single-cell data was processed with Python tools. **B)**

Representative images of lymphocyte and monocyte DiI-LDL uptake after lipid starvation. **C)**

Histogram for cellular DiI-LDL intensities in lymphocytes and monocytes **(D)** from a single

well. **E)** Quantification of mean DiI-LDL intensities and DiI-LDL organelles **(F)** in lymphocytes

(Ly) and monocytes (Mo); representative of eight independent experiments, each with four wells

per treatment; Student's t-test. **G)** Representative images of DiI-LDL uptake in monocytes

isolated from FH patients with *LDLR* mutations Cys325Tyr or Ser580Phe and a control after

lipid starvation. **H)** Quantification of monocyte (Mo) and lymphocyte (Ly) cellular DiI-LDL

intensities (Int), DiI-LDL organelle numbers (No) and pan-uptake; duplicate wells / patient

(eight wells / patient for pan-uptake). Significant changes to control 2 were calculated with

Welch's t-test. *** $p < 0.001$, ** $p < 0.01$, scale bar = 10 μm , error bars = SEM.

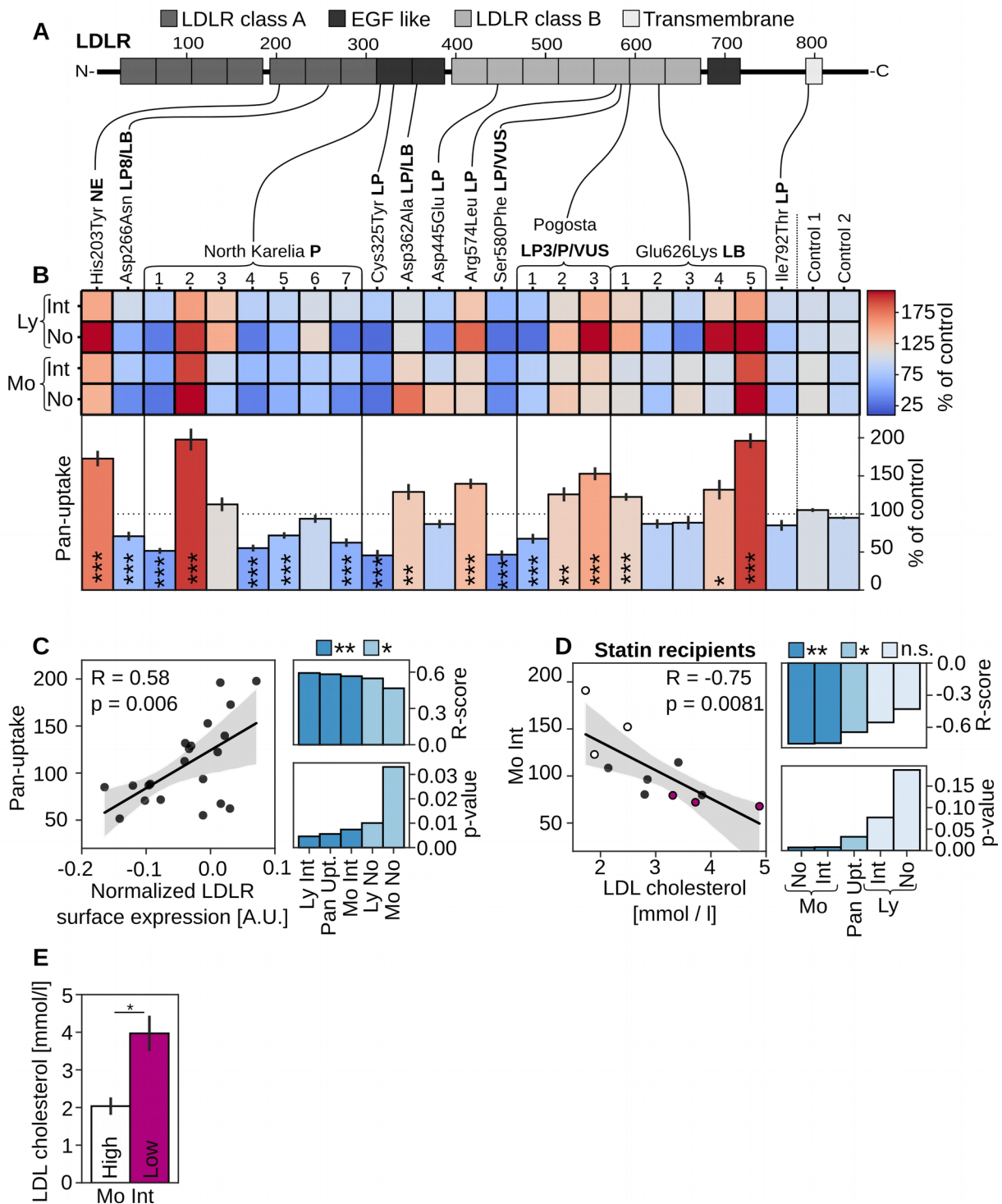


Figure 2) Heterogeneous LDL uptake and LDLR surface expression in He-FH patients'

monocytes. A) Schematic presentation of *LDLR* mutations included in this study together with

their pathogenicity status from ClinVar and LOVD databases. (P = pathogenic, LP = likely pathogenic, LB = likely benign, VUS = variant of unknown significance. **B**) Quantification of monocyte (Mo) and lymphocyte (Ly) cellular DiI-LDL intensities (Int), organelle numbers (No) and pan-uptake normalized to two controls (100%); two to three independent experiments, each with duplicate or quadruplicate wells per patient (8-16 wells per patient for pan-uptake), Cys325Tyr and Ser580Phe were described in (**Figure 1G, H**). Significant changes to control two were calculated with Welch's t-test. **c**) Correlation of pan-uptake and monocyte LDLR surface expression, including R- and p-values for all uptake scores; n = 21 patients. **D**) Correlation of monocyte DiI-LDL intensities (Mo Int) with circulating LDL-cholesterol (LDL-c) for heterozygous FH patients on statin monotherapy, including R- and p-values for all uptake scores. **E**) LDL-c concentration for 3 patients with the highest (high) and lowest (low) monocyte mean DiI-LDL intensity (Mo Int) as in **D**. Grey areas in scatter plots indicate 95% CI, *p<0.05, ** p<0.01, *** p<0.001.

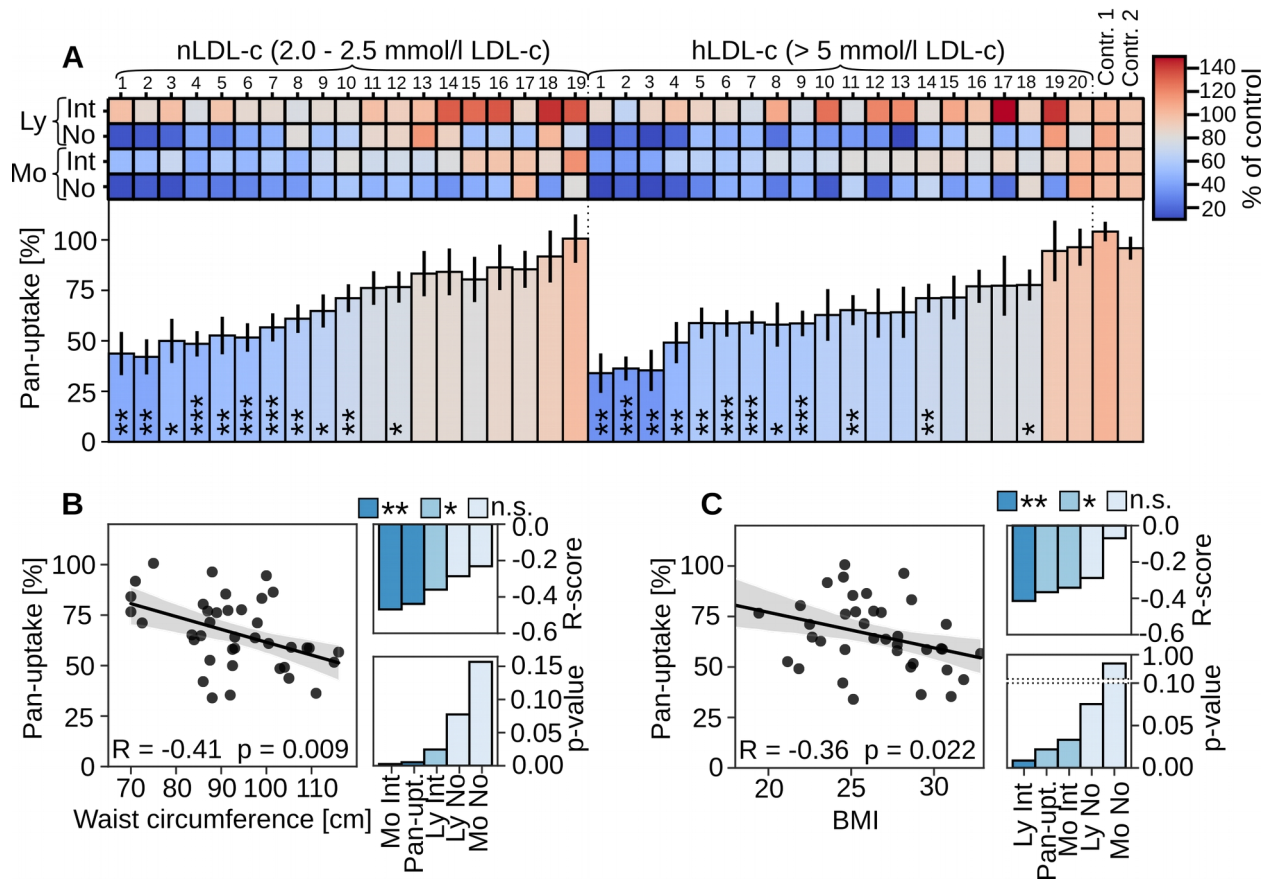


Figure 3) LDL uptake profiles in non-FH individuals with normal and elevated LDL-c. A)

Quantification of monocyte (Mo) and lymphocyte (Ly) mean DiI-LDL intensities (Int), organelle numbers (No) and pan-uptake after lipid starvation, normalized to control standards; duplicate wells per patient (eight wells per patient for pan-uptake). Significant changes to control two were calculated with Welch's t-test. **B)** Correlation of pan-uptake with waist circumference and **C)** with body mass index (BMI), including R- and p-values for all uptake scores. n = 39. Grey areas in scatter plots indicate 95% CI. * $p < 0.05$, ** $p < 0.01$, *** $p < 0.001$.

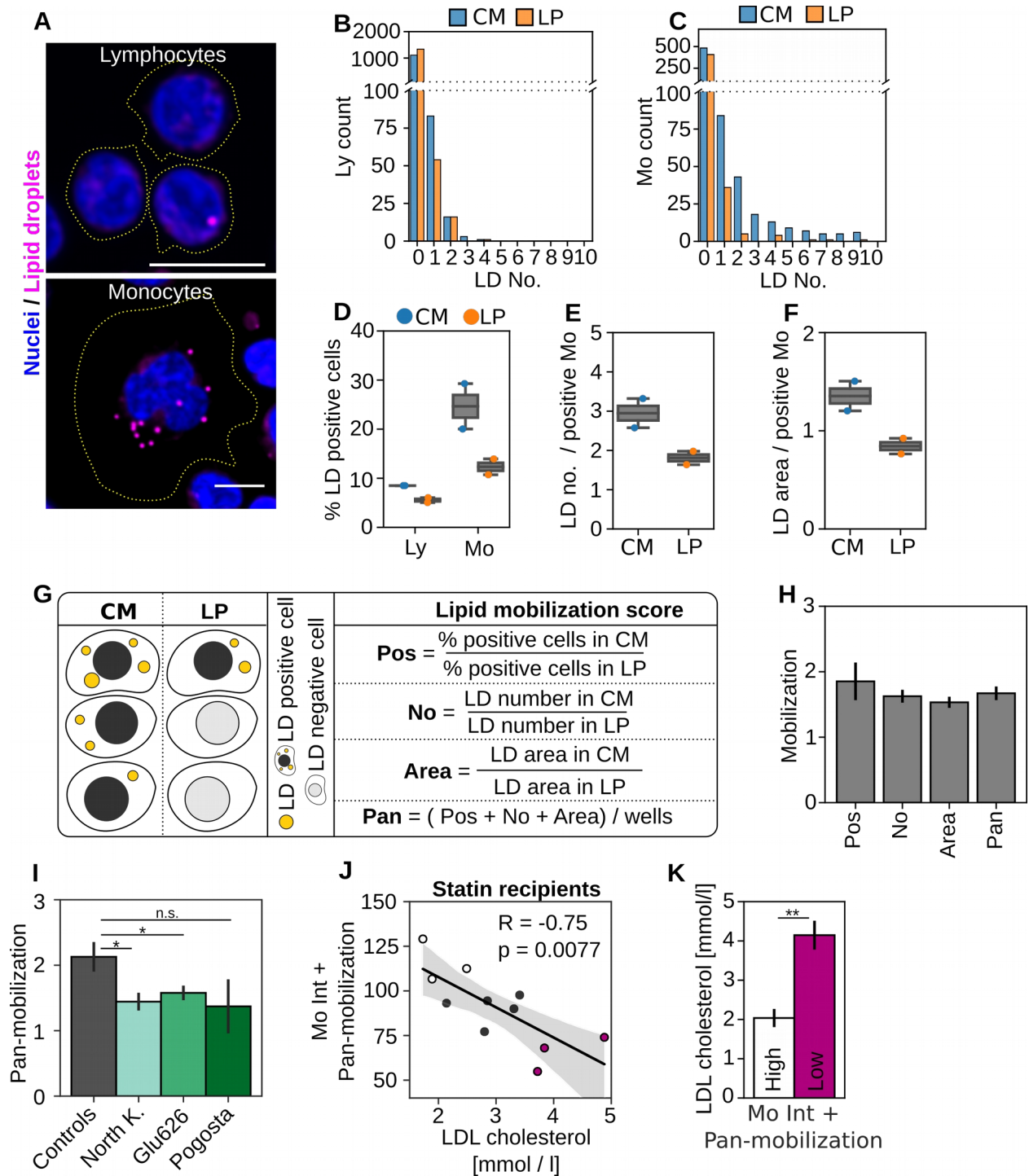


Figure 4) Lipid mobilization assay. A) Representative images showing lipid droplets (LDs) in lymphocyte and monocyte populations after treatment with control medium, scale bar = 10 μ m.

B) Histogram for cellular LD counts in lymphocyte and **(C)** monocyte populations after treatment with control medium (CM) and lipid starvation (LP) from a single well. **D)** Quantification of LD positive cells in lymphocytes (Ly) and monocytes (Mo) upon treatment with control medium (CM) and lipid starvation (LP); representative of three independent experiments, each with duplicate wells per patient and treatment. **E)** LD counts and **(F)** total LD area in LD positive monocytes quantified for the same experiment as in **(D)**. **G)** Schematic presentation of the lipid mobilization score. Upon lipid starvation, the fraction of LD positive monocytes (LD-Pos), their total LD area (LD-Area) and LD numbers (LD-No) are decreasing. Mobilization scores are calculated by dividing the amount of LD-Pos, LD-No or LD-Area in CM with the respective quantifications after lipid starvation. Pan-mobilization is the average of LD-Pos, LD-No and LD-Area mobilization scores from individual wells. **H)** Lipid mobilization scores for one control; n = 6 wells from three independent experiments, (18 wells for pan-mobilization), \pm SEM. **I)** Pan-mobilization for controls (combined control one and two from five experiments), FH-North-Karelia (n = 7), FH-Pogosta (n = 3) and FH-Glu626 (n = 5). **J)** Correlation of combined monocyte mean DiI-LDL intensities (Mo Int) and pan-mobilization with circulating LDL-c. **K)** LDL-c concentration for 3 patients with the highest (high) and lowest (low) combined score as in **J**. *p < 0.05, **p < 0.01

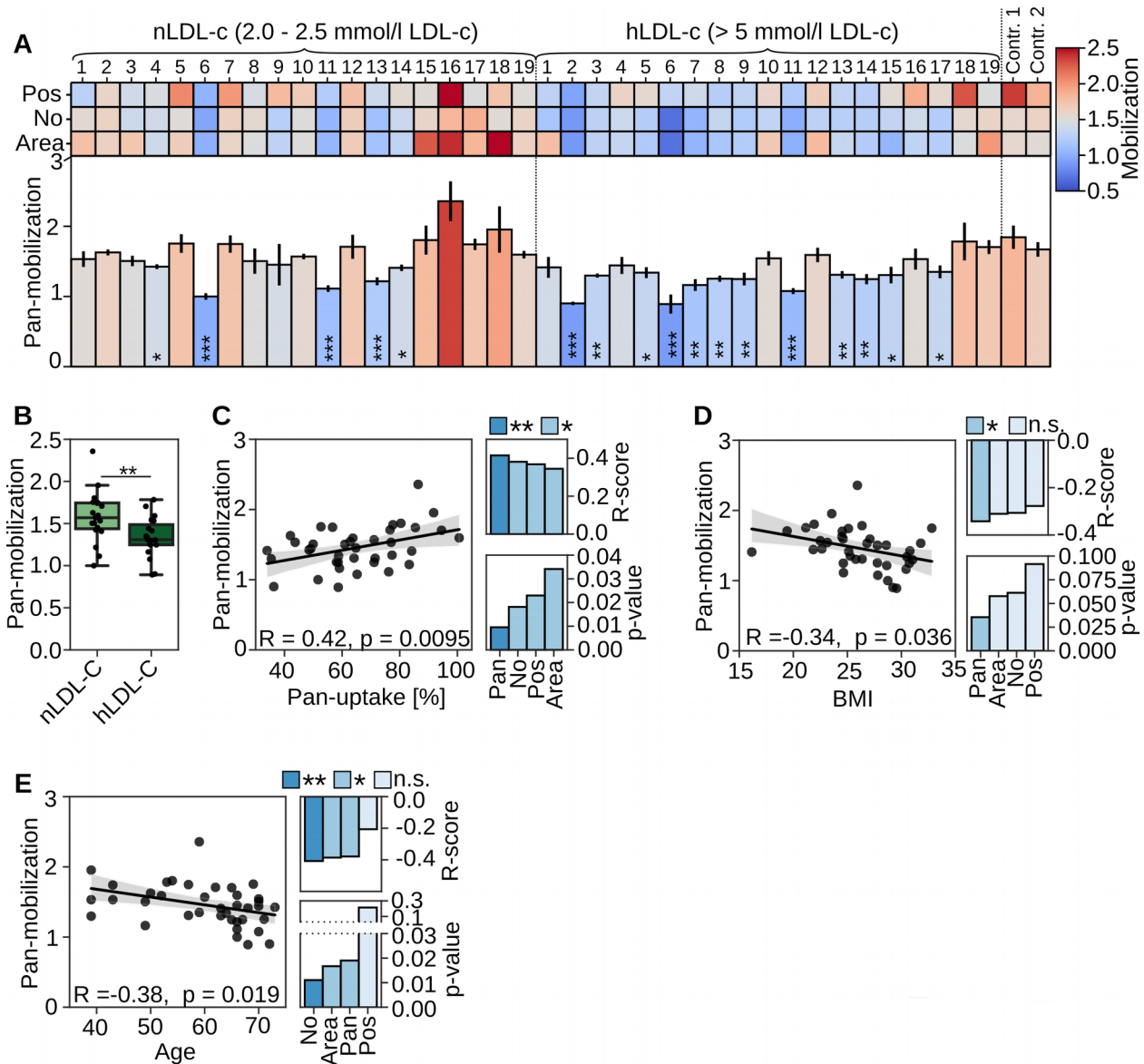


Figure 5) Monocyte lipid mobilization correlates with LDL uptake and is reduced in subjects with elevated LDL-c. A) Mobilization scores (Pos, LD-No, LD-Area and pan-mobilization) in monocytes from controls (nLDLc, LDL-c 2-2.5 mmol/l) and individuals with elevated LDL-c (hLDL-c, LDL > 5 mmol/l) sorted according to the pan-uptake score (**Figure 3A**); duplicate wells per patient (six wells per patient for pan-mobilization). Significant changes to control two were quantified with Welch's t-test. **B)** Box plot of pan-mobilization for nLDL-c

and hLDL-c subgroups; nLDL-c n = 19, hLDL-c n = 19. ** p < 0.01, Students t-test. Correlation of pan-mobilization with pan-uptake (**C**), BMI (**D**) and age (**E**) including R- and p-values for all mobilization scores. Grey areas in scatter plots = 95% CI. * p<0.05, * p<0.01, *p<0.001.

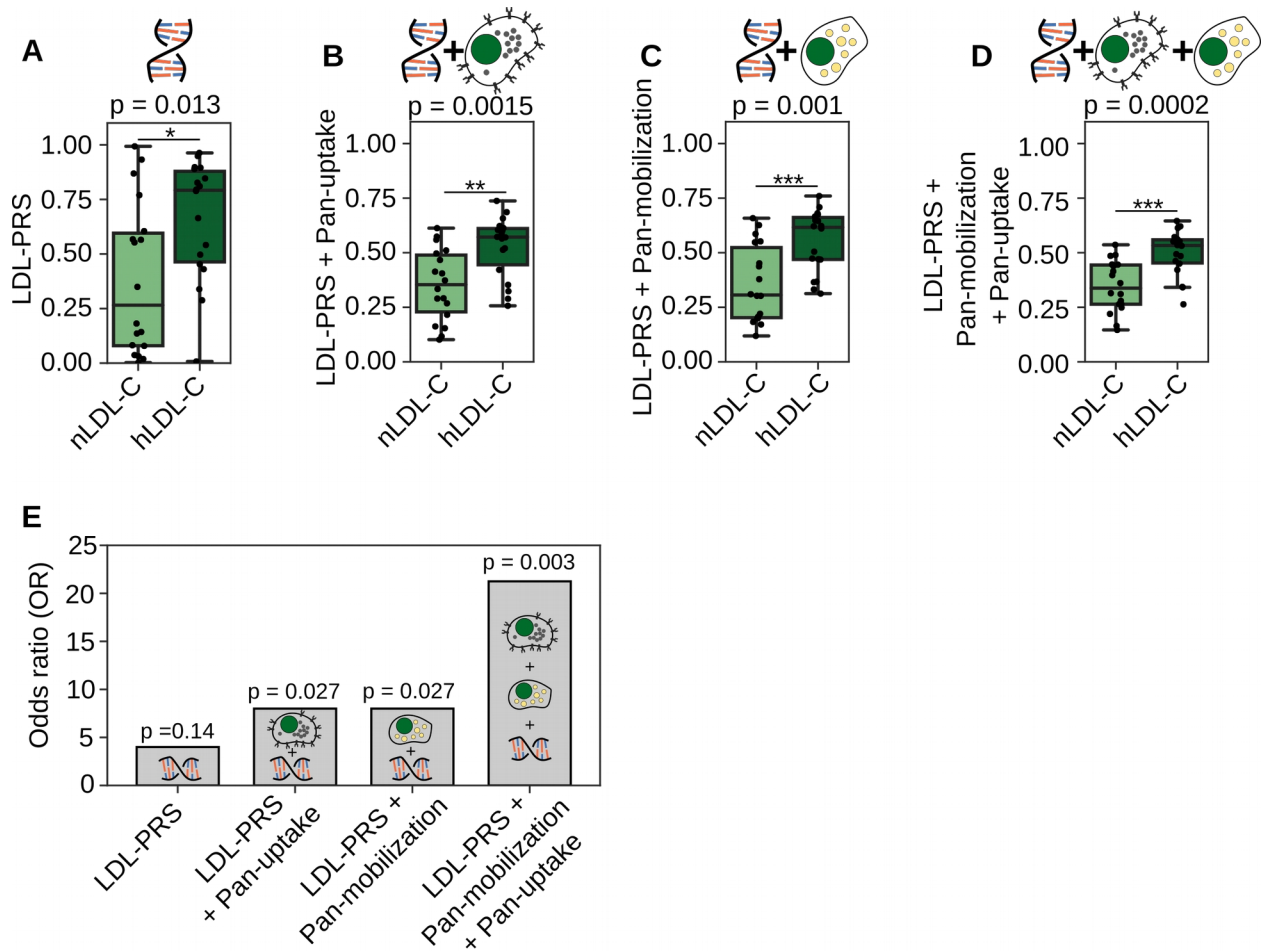


Figure 6) Hybrid scores combining genetic and functional cell based data show improved association with hypercholesterolemia. A) Box plot of a polygenic risk score for high LDL-c levels (LDL-PRS) for nLDL-c (2-2.5 mmol/l LDL-c) and hLDL-c (>5 mmol/l LDL-c) subgroups. **B)** Box plot for double hybrid scores combining LDL-PRS and pan-uptake or pan-mobilization **(C)** into a single score. **D)** Box plot for a triple hybrid score consisting of LDL-PRS, pan-uptake and mobilization. nLDL-c n = 18, hLDL-c n = 19, * $p < 0.05$, ** $p < 0.01$, *** $p < 0.001$; Welch's t-test. **E)** Odds ratio (OR) for 30% of the individuals with the highest LDL-PRS, double or triple hybrid scores and the remaining subjects, calculated with the Fisher's exact probability test.

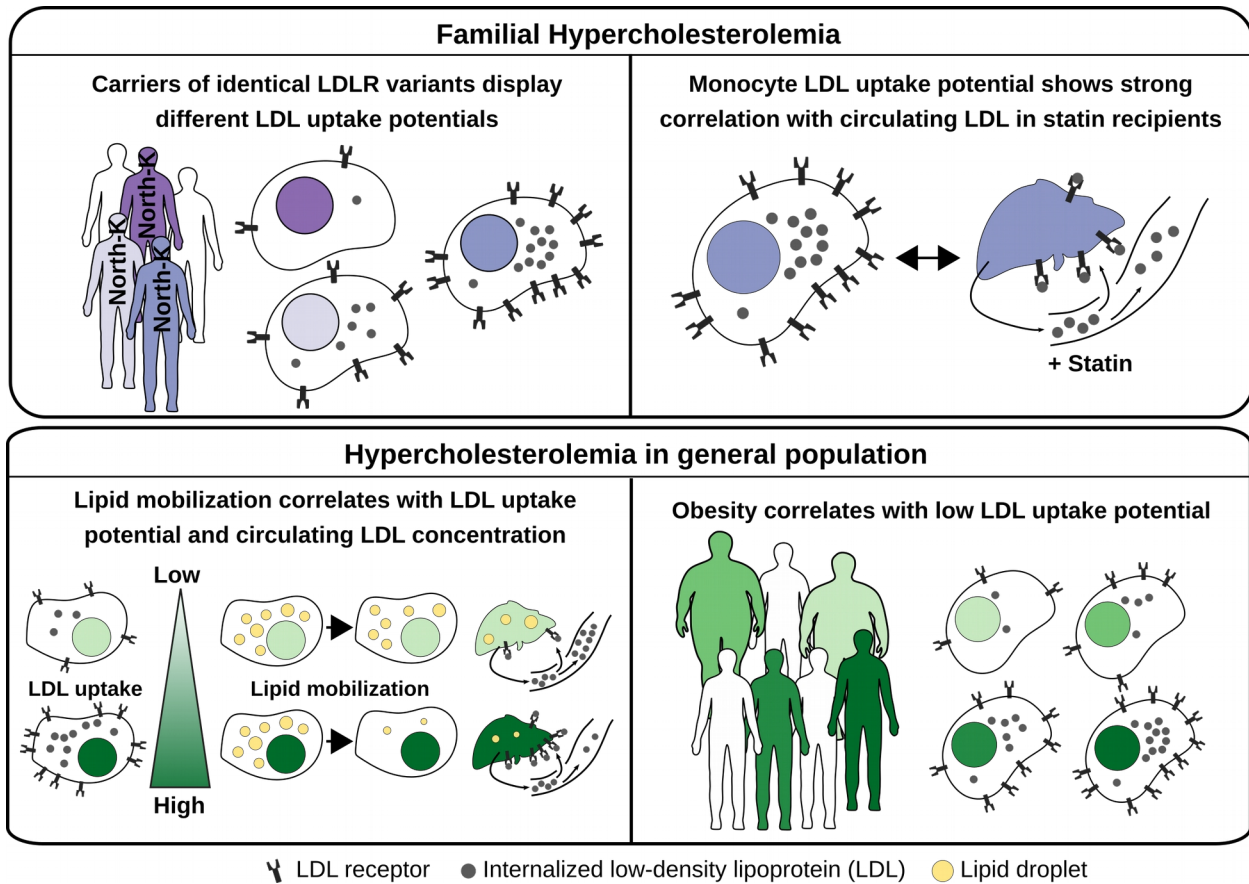


Figure 7) Schematic illustration of functional readouts in peripheral blood mononuclear cells and their correlation with physiological outcomes in monogenic and polygenic hypercholesterolemia.